



HAL
open science

Time-lapse magnetic resonance sounding measurements for numerical modeling of water flow in variably saturated media

Anatoly Legchenko, Jean-Michel Baltassat, Céline Duwig, Marie Boucher,
Jean-François Girard, Alvaro M Soruco, Alain Beauce, Francis Mathieu,
Cédric Legout, Marc Descloitres, et al.

► To cite this version:

Anatoly Legchenko, Jean-Michel Baltassat, Céline Duwig, Marie Boucher, Jean-François Girard, et al. Time-lapse magnetic resonance sounding measurements for numerical modeling of water flow in variably saturated media. *Journal of Applied Geophysics*, 2020, 175, pp.103984. 10.1016/j.jappgeo.2020.103984 . hal-02913622

HAL Id: hal-02913622

<https://brgm.hal.science/hal-02913622>

Submitted on 5 Dec 2022

HAL is a multi-disciplinary open access archive for the deposit and dissemination of scientific research documents, whether they are published or not. The documents may come from teaching and research institutions in France or abroad, or from public or private research centers.

L'archive ouverte pluridisciplinaire **HAL**, est destinée au dépôt et à la diffusion de documents scientifiques de niveau recherche, publiés ou non, émanant des établissements d'enseignement et de recherche français ou étrangers, des laboratoires publics ou privés.

1 **Time-lapse Magnetic Resonance Sounding measurements for numerical**
2 **modeling of water flow in variably saturated media**

3

4 Anatoly Legchenko¹, Jean-Michel Baltassat², Céline Duwig¹, Marie Boucher¹, Jean-François Girard³,
5 Alvaro Soruco⁴, Alain Beauce², Francis Mathieu², Cedric Legout⁵, Marc Descloitres¹ and Gabriela
6 Patricia Flores Avilés⁴

7 1. Univ. Grenoble Alps, Institute of Research for Development, IGE, Grenoble, France,

8 E-mail: anatoli.legtchenko@ird.fr

9 2. BRGM, Orléans, France

10 3. IPGS/EOST, Strasbourg University, France

11 4. Instituto de Investigaciones Geológicas y del Medio Ambiente, Universidad Mayor de
12 San Andrés, La Paz, Bolivia

13 5. Univ. Grenoble Alps, IGE, France

14 **ABSTRACT**

15 We presented an innovative hydrogeophysical approach that allows numerical modeling of
16 water flow in a variably saturated media. In our model, we approximated the subsurface by
17 horizontally stratified porous media. The model output was a time varying water content
18 profile. Then, we compared the water content provided by the model with the water content
19 measurements carried out using the time-lapse Magnetic Resonance Sounding (MRS) method.
20 Each MRS sounding provided a water content profile in the unsaturated zone down to twenty
21 meters. The time shift between the profiles corresponded to the time lapse between individual
22 MRS soundings. We minimized the discrepancy between the observed and the modeled MRS
23 signals by varying hydraulic parameters of soil layers in the water flow model. For measuring
24 and processing MRS data, we used NUMIS MRS instrument and SAMOVAR software. We
25 carried out water flow modeling with HYDRUS-1D software. This paper reports our results
26 and summarizes the limitations of the MRS method applied to water content measurements in
27 the unsaturated zone.

28 *Keywords:* MRS, hydrodynamic modeling, time-lapse, Villamblain, Beauce

29 INTRODUCTION

30 Sustainable management of water resources, estimation of aquifers recharge and expansion of
31 water protection measures require development of numerical models representing these
32 hydrological processes. The classification of hydrological models is not exact, and many
33 models may have overlapping features. For describing similar processes, different models can
34 be appropriate (*Jajarmizadeh et al., 2012; Sood and Smakhtin, 2015*). The complexity of any
35 hydrological model depends on the objectives of the modeling work, the complexity of the
36 subsurface, and the experimental data. In each case, it is necessary to find a compromise
37 between modeling accuracy and completeness of the data set. In all cases, the heterogeneity of
38 the subsurface and consequent heterogeneity of soil hydraulic properties represent a major
39 difficulty for accurate numerical modeling. For modeling, one needs to know these
40 heterogeneities and the surface geophysical methods are often used (*Rubin and Hubbard,*
41 *2006; Binley et al., 2015*). Among them, the Ground Penetrating Radar (GPR) and the
42 Electrical Resistivity Tomography (ERT) are the most popular. These methods identify
43 different geological patterns and exploit correlations between the electrical and hydraulic
44 properties of the subsurface (e.g., *Kemna et al., 2002; Kowalski et al., 2004; Camporese et al.,*
45 *2012; Carrière et al., 2013; Høyer et al., 2015; Vereecken et al., 2015; Carrière et al., 2016;*
46 *Park et al., 2017; Jouen et al., 2018; Power et al., 2018; Saito et al., 2018; Ikard and Pease,*
47 *2019*). However, other physical properties of soils also affect electrical conductivity. The
48 most common of them is the clay content. Thus, the electrical conductivity dependent on
49 many factors, which can render uncertain interpretation of field measurements in terms of
50 groundwater.

51 The Magnetic Resonance Sounding (MRS) also known as the Surface Nuclear Magnetic
52 Resonance (SNMR) is a geophysical method sensitive to liquids that contain hydrogen (oil,
53 water). The phenomenon of nuclear magnetic resonance (NMR) is the physical basis of MRS

54 (e.g., *Legchenko and Valla, 2002; Roy and Lubczynski, 2003; Lubczynski and Roy, 2004;*
55 *Hertrich, 2008; Legchenko, 2013; Chevalier et al., 2014; Behroozmand et al., 2015;*
56 *Garambois et al., 2016; Legchenko et al., 2017*). At shallow depth, only water produces
57 measurable MRS signal, and interpretation of MRS measurements in terms of water is
58 unambiguous. It is a competitive advantage of this method. Under ideal theoretical conditions,
59 the amplitude of the MRS signal is proportional to the quantity of water in the subsurface.
60 However, the accuracy of the MRS method depends on the accuracy of MRS measurements
61 and inversion. The complexity of soil structures may affect MRS measurements and
62 calibration of MRS results using other metrological means can improve the accuracy. For
63 example, an aquifer test by pumping can allow calibrating the MRS water content under
64 saturation (*Vouillamoz et al., 2013*). The water content measured in a borehole (neutron log or
65 NMR log, for example) or in a laboratory on rock samples allow calibration of the unsaturated
66 water content. The principal application of MRS is the localization and characterization of
67 aquifers (specific yield, hydraulic conductivity) (e.g., *Legchenko et al., 2002; Lubczynski and*
68 *Roy, 2003; Vouillamoz et al., 2005; 2008; 2012; Chalikakis et al., 2008; Boucher et al., 2009;*
69 *Favreau et al., 2009; Müller-Petke et al., 2011; Nielsen et al., 2011; Vilhelmsen et al., 2014;*
70 *Valois et al., 2018*). Some papers report the use of MRS for constraining water flow modeling
71 aiming to reduce uncertainty in the model parameters (*Lubczynski and Gurwin, 2005;*
72 *Boucher et al., 2009; 2012; Chaudhuri et al., 2013; Baroncini-Turricchia et al., 2014; Comte*
73 *et al., 2018*). The MRS can estimate the water content also in the unsaturated zone (*Roy and*
74 *Lubczynski, 2005; Costabel and Yaramanci, 2011; Walsh et al., 2014; Falzone and Keating,*
75 *2016*) and contribute to water content monitoring (*Descloitres et al., 2008; Legchenko et al.,*
76 *2008; Herckenrath et al., 2012; Legchenko et al., 2014*).

77 In this paper, we presented results of a methodological study carried out with the goal to
78 investigate the possibility of combining time-lapse MRS measurements with a water flow

79 modeling in variably saturated media. For developing the unsaturated water flow model, we
80 used MRS time-lapse measurements of the water content in the unsaturated zone. MRS
81 averages the water content over the volume investigated with the MRS loop thus defining the
82 scale of the water flow modeling. We build a model using available software based on the
83 Richards equation (HYDRUS-1D). This model aimed to reproduce time varying water
84 content observed with the MRS. Because of the subsurface in the investigated area is
85 heterogeneous the hydraulic parameters of the synthetic layers in our model may not
86 correspond to the hydraulic parameters of the real subsurface and did not represent the target
87 for the hydraulic modeling.

88 **BACKGROUND**

89 *Numerical modeling of the water flow in variably saturated media*

90 For describing the one - dimensional vertical water flow, we used Richards equation

$$91 \quad \frac{\partial \theta(h)}{\partial t} = \frac{\partial}{\partial z} \left[K(h) \frac{\partial h}{\partial z} - K(h) \right], \quad (1)$$

92 where h is the negative of the matric potential, θ is the volumetric water content, and K is
93 the unsaturated hydraulic conductivity. For solving Richards equation, we represented the soil
94 water retention function $\theta(h)$ and the unsaturated hydraulic conductivity $K(h)$ in the
95 functional form using a hydraulic property model (e.g., *Campbell*, 1974; *van Genuchten*,
96 1980; *Durner*, 1994; *Kosugi*, 1994; *Poulsen et al.*, 2002). All reported models are
97 approximations that represent real soils with limited accuracy (*Madi et al.*, 2018). Under field
98 conditions, accuracy of in situ time-lapse measurements may be not sufficient for observation
99 of small differences in the water retention functions of different patterns and any of these

100 models is suitable for our study. We used the log-normal distribution model allowing faster
 101 computing when using HYDRUS-1 software (Kosugi, 1996)

$$102 \quad S_e = \frac{\theta - \theta_r}{\theta_s - \theta_r} = \begin{cases} \frac{1}{2} \operatorname{erfc} \left[\frac{\ln(h/h_0)}{\sqrt{2}\sigma} \right], & (h < 0) \\ 1, & (h \geq 0) \end{cases} . \quad (2)$$

103 where S_e is the effective water content, erfc is the complementary error function, h_0 is the
 104 median metric head, $\sigma > 0$ denotes the standard deviation of the log-transformed soil pore
 105 radius and characterizes the width of the pore-size distribution.

106 The unsaturated hydraulic conductivity is (Mualem, 1976)

$$107 \quad K(h) = \begin{cases} K_s S_e^l \left[\frac{1}{2} \operatorname{erfc} \left[\frac{\ln(h/h_0)}{\sqrt{2}\sigma} + \frac{\sigma}{\sqrt{2}} \right] \right]^2, & (h < 0) \\ K_s, & (h \geq 0) \end{cases} , \quad (3)$$

108 where K_s is the saturated hydraulic conductivity and l is the pore connectivity parameter.

109 Both the water content and the hydraulic conductivity are scale dependent parameters.

110 ***Magnetic Resonance Sounding***

111 MRS is a geophysical method designed for non-invasive measurements of water content in
 112 the subsurface (Legchenko, 2013). For measuring, we used a wire loop on the surface. In this
 113 loop, we generated a pulse of alternating current with the amplitude I_0 and duration τ . The
 114 frequency of the current was equal to the resonance frequency of proton spins in the Earth's

115 magnetic field $f_0 = \omega_0 / 2\pi$ (Larmor frequency). After we cut the current off, hydrogen
 116 protons in the liquid phase generate an electromagnetic field also oscillating at the Larmor
 117 frequency. The resonance behavior of protons in the Earth's magnetic field renders the
 118 method sensitive to water in the subsurface. MRS measurements average the results over the
 119 volume defined by the size of the loop. The loop may cover the surface area of $2a \times 2a$ m²
 120 where a is the side length of a square loop (Legchenko *et al.*, 1997). Typical loop sizes vary
 121 from 10×10 to 150×150 m². Using a smaller loop (2×2 m²) one can improve the lateral
 122 resolution. However, it also reduces the depth of investigation (Lin *et al.*, 2016; Grombacher
 123 *et al.*, 2018). With any loop, the depth of investigation depends on the electrical conductivity
 124 of the subsurface (Legchenko *et al.*, 1997).

125 We computed the initial amplitude of the MRS signal using the following integral equation
 126 (Legchenko and Valla, 2002)

$$127 \quad e(q) = \frac{\omega_0}{I_0} \int_V B_1 M_0 \sin\left(\frac{\gamma B_1 q}{2I_0}\right) \tilde{\theta} dV, \quad (4)$$

128 where $\omega_0 = \gamma B_0$, γ is the gyromagnetic ratio for protons, B_0 is the magnitude of the Earth's
 129 magnetic field, M_0 is the equilibrium spin magnetization per unit volume, $q = I_0 \tau$ is the
 130 pulse moment, B_1 is the component of the transmitted magnetic field transverse to the
 131 Earth's magnetic field and $\tilde{\theta}$ is the volumetric water.

132 We got the electrical conductivity of the subsurface and the Larmor frequency using other
 133 than MRS geophysical measurements and considered the MRS inversion as a linear inverse

134 problem. For inversion, we assumed the subsurface horizontally stratified and approximated
 135 the integral equation (4) by a system of algebraic equations

$$136 \quad \mathbf{A}\tilde{\boldsymbol{\theta}} = \mathbf{e}, \quad (5)$$

137 where $\mathbf{A} = [a_{i,j}]$ is a rectangular matrix, $\mathbf{e} = [e_i]$ and $\tilde{\boldsymbol{\theta}} = [\tilde{\theta}_j]$ are the set of experimental

138 data and the solution vector, $i=1,2,\dots,I$ is the number of pulse moments, and $j=1,2,\dots,J$ is the
 139 number of model layers in the solution vector. We computed the matrix \mathbf{A} by discretizing the

140 Eq. 4. First, we estimated the maximum depth of investigation of the method z_{\max} , which

141 depends on the loop size and the measuring conditions (Legchenko et al., 1997). Then, we

142 represented the subsurface by homogeneous horizontal layers of the thickness $\Delta\tilde{z}_j$ so that

143 $\Delta\tilde{z}_j \leq \Delta\tilde{z}_{j+1}$ and $\sum_{j=1}^J \Delta\tilde{z}_j = z_{\max}$. So, each column of the matrix \mathbf{A} contained the amplitude of the

144 magnetic resonance signal versus pulse moment computed considering the corresponding

145 layer $\Delta\tilde{z}_j$ (Legchenko and Shushakov, 1998).

146 Different mathematical methods allow estimating the resolution of an inverse problem. The

147 most common is the singular value decomposition (SVD) (Aster et al., 2012). Many studies

148 have reported application of the of SVD to the MRS inversion (e.g., Weichman et al., 2002;

149 Müller-Petke and Yaramanci, 2008; Legchenko and Pierrat, 2014). Other methods like

150 Monte-Carlo simulations (Guillen and Legchenko, 2002a; Chevalier et al., 2014; Andersen et

151 al., 2018), linear programming (Guillen and Legchenko, 2002b) and bootstrap statistics

152 (Parsekian and Grombacher, 2015) also proved their efficiency. A joint use of different

153 methods can improve the reliability of the results. For example, Legchenko et al. (2017)

154 combined the SVD and the Monte-Carlo methods. For solving the Eq. 5, one may apply the

155 well-known algorithms (e.g., *Guillen and Legchenko, 2002a; 2002b; Mohnke and Yaramanci,*
 156 *2002; Müller-Petke and Yaramanci, 2010; Behroozmand et al., 2012; Chevalier et al., 2014;*
 157 *Irons and Li, 2014*). We use the Tikhonov regularization method (*Legchenko and Shushakov,*
 158 *1998*), which assumes a smoothness of the water content profile (*Tikhonov and Arsenin,*
 159 *1977*). Thus, the solution of the Eq. 6 approximates the solution of the Eq. 5

$$160 \quad \min_{\tilde{\theta}} \left(\left\| \mathbf{A}\tilde{\theta} - \mathbf{e} \right\|_{L_2} + \alpha_z \times \left\| \frac{\partial}{\partial z} \tilde{\theta} \right\|_{L_2} \right), \quad (6)$$

161 considering the Eq. 7

$$162 \quad \left\| \mathbf{A}\tilde{\theta} - \mathbf{e} \right\|_{L_2} \leq \varepsilon. \quad (7)$$

163 where α_z is the smoothing factor and ε is an experimental error.

164 The water contents $\tilde{\theta}_j$ and the thickness of model layers $\Delta\tilde{z}_j$ allowed us estimating the
 165 equivalent water column H_w . H_w is a more stable parameter than $\tilde{\theta}_j$ or $\Delta\tilde{z}_j$ (*Legchenko et*
 166 *al., 2004*)

$$167 \quad H_w = \sum_j \tilde{\theta}_j \Delta\tilde{z}_j. \quad (8)$$

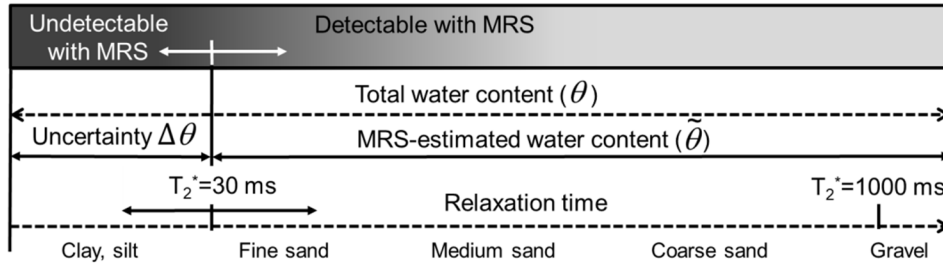
168 Another important parameter of the magnetic resonance signal is relaxation times T_1 , T_2 and
 169 T_2^* (*Dunn et al., 2002*). Measurements of the relaxation times in water saturated porous
 170 media allow estimating the mean pore size related to the hydraulic conductivity. However, the
 171 relaxation times are also sensitive to paramagnetic minerals in the subsurface that can disturb

172 the homogeneity of the Earth's magnetic field. In the case of non-magnetic rocks and a
 173 homogeneous Earth's magnetic field, T_1 and T_2^* are obtained. In this case, $T_2 = T_2^*$.
 174 Magnetic materials render the Earth's magnetic field heterogeneous and all three relaxation
 175 times (T_1 , T_2^* and T_2) can be measured. In water saturated porous media, only the
 176 relaxation times T_1 (Seevers, 1966) or T_2 (Kenyon, 1997) allow reliable estimation of the
 177 saturated hydraulic conductivity. These estimates show good results also when applied with
 178 MRS (Schirov *et al.*, 1991; Legchenko *et al.*, 2004; Legchenko *et al.*, 2010; Vouillamoz *et al.*,
 179 2011). However, the unsaturated hydraulic conductivity is a non-linear function of the water
 180 content and the estimates developed for water saturated porous media provide acceptable
 181 results only when the unsaturated media is close to saturation.

182 We used an instrument developed by IRIS Instruments in 1996 (NUMIS) and designed for
 183 detecting water in the subsurface with $T_2^* > 30$ ms. Recent MRS instruments allow measuring
 184 the MRS signals with $T_2^* > 10$ ms (Walsh, 2008), but measurements of a short signal are
 185 always difficult. Undetectable water causes an underestimation of the water content $\Delta\theta$
 186 (Legchenko *et al.*, 2004)

$$187 \quad \begin{cases} \tilde{\theta} = \theta - \Delta\theta & \text{if } \theta > \Delta\theta \\ \tilde{\theta} = 0 & \text{if } \theta \leq \Delta\theta \end{cases} \quad (9)$$

188 For example, in clay $T_2^* < 30$ ms and the water content estimated with MRS is close to zero (
 189 $\tilde{\theta} = 0$). In coarse material (sand, gravel), $\Delta\theta \rightarrow 0$ and in bulk water $\Delta\theta = 0$. Fig. 1 shows
 190 the capacity of MRS to detect water in different geological materials.



191

192 *Figure 1. Schematic presentation of the MRS capacity to measure the water content in water*
 193 *saturated porous media. Examples of geological material that correspond to the increasing*
 194 *pore size.*

195

196 The threshold of $T_2^* = 30$ ms between a low permeable material (silt, clay) and a permeable
 197 material (fine sand) is not a constant. It depends on the magnetic susceptibility and the surface
 198 relaxivity rate of the geological formation. For example, we have two types of material with
 199 the same hydraulic properties and different magnetic susceptibilities and/or surface relaxivity
 200 rates. In the first material with higher magnetic susceptibility (and/or surface relaxivity rate),
 201 T_2^* is shorter than that in the second material and $T_2^* = 30$ ms can correspond to fine sand.

202 The same value of $T_2^* = 30$ ms can correspond to silt or clay in the second material. The
 203 volume of water producing the MRS signal with $T_2^* < 30$ ms depends on the material and
 204 hence, the threshold between detectable and undetectable with MRS water is not a constant. It
 205 renders the uncertainty $\Delta\theta$ site dependent (Legchenko et al., 2004). However, the time-lapse
 206 procedure comprises measurements in the same material and hence, $\Delta\theta$ is a systematic error.

207 In many materials, $\Delta\theta > \theta_r$, which does not allow measuring with the MRS the initial part of
 208 the water retention function.

209 For each individual sounding, the Tikhonov regularization (Eq. 6) assumes a smoothness of
 210 the water content profile. When processing time-lapse measurements, we added the
 211 smoothness constraint versus time. Thus, the time-lapse MRS inversion required solving the
 212 following equation

$$213 \quad \min_{\tilde{\boldsymbol{\theta}}} \left(\left\| \mathbf{A}\tilde{\boldsymbol{\theta}} - \mathbf{e} \right\|_{L2} + \alpha_z \times \left\| \frac{\partial \tilde{\boldsymbol{\theta}}}{\partial z} \right\|_{L2} + \alpha_t \times \left\| \frac{\partial \tilde{\boldsymbol{\theta}}}{\partial t} \right\|_{L2} \right) < \varepsilon, \quad (10)$$

214 where α_z, α_t are the smoothing factors. The matrix \mathbf{A} has $I = L \times K$ rows and
 215 $J = M \times K$ columns, where K is the number of time-lapse soundings ($k=1,2,\dots,K$), L is
 216 the number of the pulse moments per sounding ($l=1,2,\dots,L$), and M is the number of layers
 217 per sounding in the inverse model ($m=1,2,\dots,M$).

218 **Unsaturated water flow modeling using MRS data**

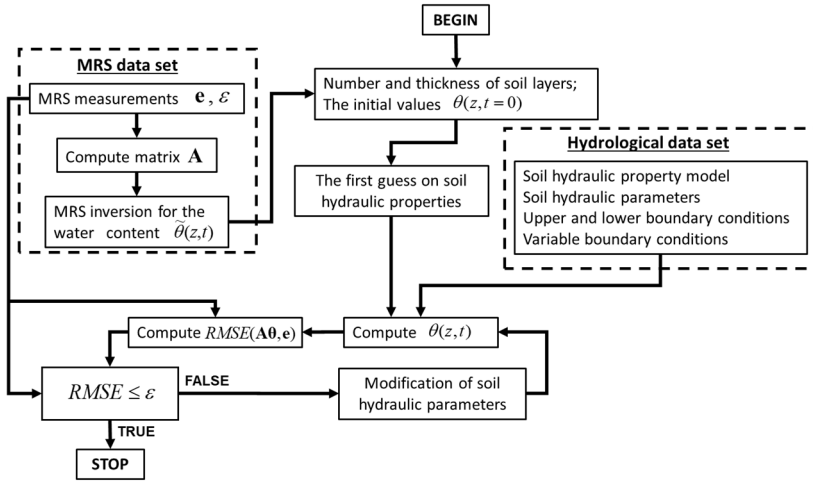
219 We calibrated the water flow model by minimizing the discrepancy between the theoretical
 220 and the experimental MRS signals

$$221 \quad \min_{\boldsymbol{\theta}} \left(\left\| \mathbf{A}\boldsymbol{\theta} - \mathbf{e} \right\|_{L2} \right) < \varepsilon, \quad (11)$$

222 where \mathbf{e} is the measured amplitude of the MRS signal, $\boldsymbol{\theta}$ is the water content provided by the
 223 water flow model, and ε is an experimental error. We estimated the discrepancy between the
 224 theoretical and experimental data with the root-mean-square error

$$225 \quad RMSE = \sqrt{I^{-1} \sum_{i=1}^I \sum_{j=1}^J (a_{i,j} \theta_j - e_i)^2} \leq \varepsilon. \text{ Fig. 2 shows the flowchart of the inverse modeling}$$

226 procedure.



227

228 *Figure 2. The flowchart of the inverse modeling procedure.*

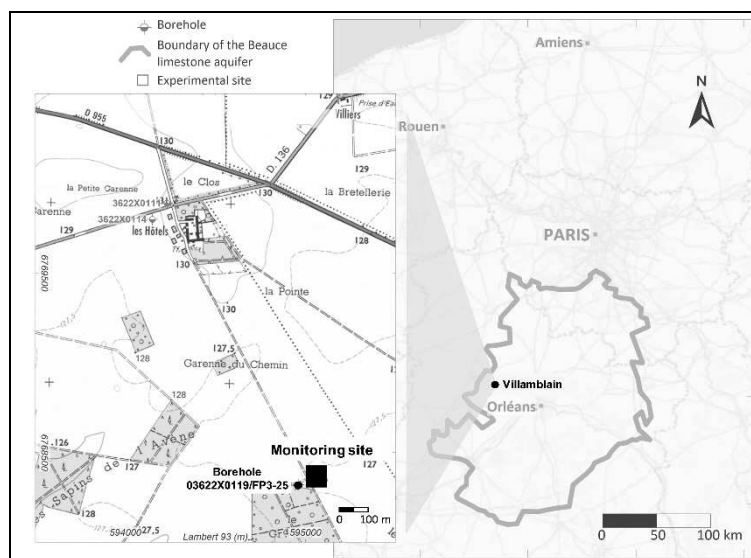
229

230 In the Fig. 2, the MRS data set comprised the measured amplitude of the MRS signal and the
 231 matrix \mathbf{A} . Field measurements also provided an estimate of the experimental error. For
 232 computing the matrix \mathbf{A} , we considered the measuring conditions (the Earth's magnetic field
 233 and the resistivity of the subsurface) and the MRS setup (loop size, pulse moments). The
 234 time-lapse MRS inversion for water content suggested four soil layers with different hydraulic
 235 parameters. These layers represented the subsurface in the hydraulic model. The hydrological
 236 data set comprised the soil hydraulic property model, the soil hydraulic parameters, the upper
 237 and lower boundary conditions, and the variable boundary conditions. The first MRS
 238 sounding provided the initial water content profile $\theta(z, t = 0) = \tilde{\theta}(z, t = 0)$. The geological
 239 formations suggested the first guess for the soil hydraulic parameters. We iteratively adjusted
 240 the water flow model aiming to minimize the discrepancy between measured and theoretical
 241 MRS signals (Eq. 11). For solving Eq. 11, we applied the Levenberg-Marquardt algorithm
 242 (Marquardt, 1963). Iterations stopped when the discrepancy become smaller than the
 243 experimental error. If the water flow model did not allow solving Eq. 11, then we revised the
 244 entire hydraulic model.

245 **RESULTS**

246 Between 26 April 1999 and 15 March 2000 the Bureau de Recherches Géologiques et
247 Minières (BRGM, France) performed a one-year monitoring of the water content in
248 Villamblain test site (Fig. 3). We used these data to investigate the possibility of the
249 unsaturated flow modeling using time-lapse MRS measurements. The data set comprised 34
250 MRS soundings at 18 different dates (Boucher *et al.*, 2003). With a few exceptions, we
251 carried out two soundings per date aiming to avoid errors due to unexpected technical
252 problems. We used the NUMIS instrument with a 75×75 m² square loop and the maximum
253 pulse moment of 12,500 A-ms. The Larmor frequency was 2011.3 Hz. The ambient
254 electromagnetic noise varied between 150 and 300 nV being larger in spring. For interpreting
255 MRS measurements, we used SAMOVAR software developed by the authors. We considered
256 the local Earth's magnetic field (47,214 nT; 63°N), and the resistivity of the subsurface
257 provided by the electrical resistivity tomography (ERT) measurements (Jodry *et al.*, 2018).
258 For the unsaturated water flow modeling, we used HYDRUS-1D software (Šimůnek *et al.*,
259 2008a; 2008b).

260 Fig. 3 shows the location map of the monitoring site.



261

262 *Figure 3. Location map of the monitoring site. The distance between the MRS loop and the*
263 *borehole 03622X0119/FP3-25 (WGS 84: Lat.-48,00683 m; Long.-1,59130 m) is 76 m.*

264

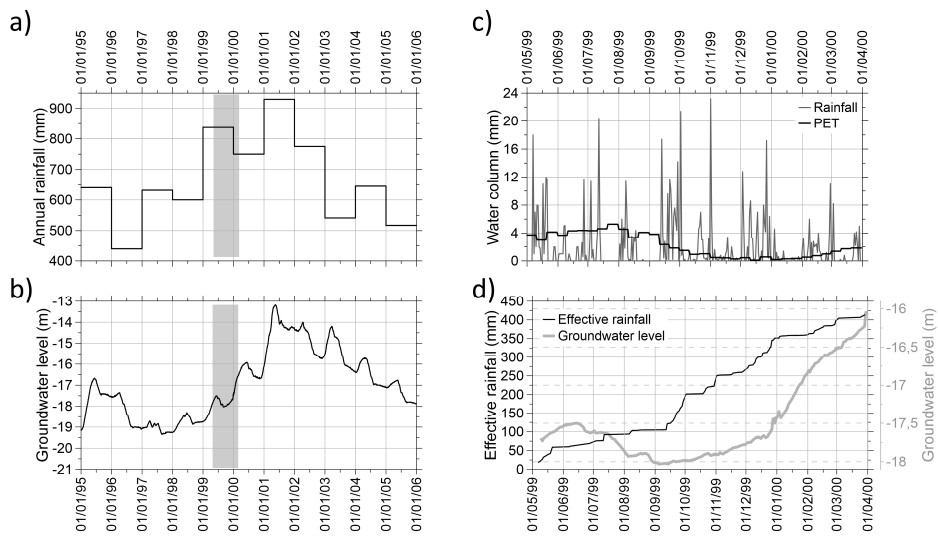
265 The Villamblain test site covers about 7 km² in the western part of the Loire River sub-
266 catchment. This area is a part of the Beauce aquifer (9,000 km²) located south-west of Paris.
267 The average altitude of the Beauce aquifer is 140 m and a regional hydraulic gradient of about
268 0.1%. The mean annual recharge is 110 mm (*Schnebelen et al.*, 1999). Developed agriculture
269 with irrigation in summer is widespread in the area (*Desprer and Megnien*, 1975; *Bruand et*
270 *al.*, 1997; *Creuzot et al.*, 1997; *Michot et al.*, 2003). In Villamblain, calcareous soils and
271 cryoturbated materials cover about 48% of the surface, Eutric Cambisols developed in loam
272 and Haplic Calcisols composed of a loamy-clay layer represent 26% and about 20%. Soil
273 thickness ranges from 0.3 to 1.5 m. The water column in these soils varies between 50 and
274 180 mm. The limestone underlying the soil layer is heterogeneous with the variable fracturing
275 and irregular karst development. Estimations of the specific yield of the limestone show 3 to
276 13% (*Bourennane et al.*, 1998; *Chéry et al.*, 1999). All the studies show no-run-off in
277 Villamblain.

278 During our study, we measured the GWL in the borehole 03622X0119/FP3-25. The
279 Villampuy weather station at 4 km from Villamblain (Lat.-48°02'18"N; Long.-1°29'30"E)
280 provided the daily rainfall data. Figures 4a and 4b show the annual rainfall and the
281 groundwater level (GWL) variations between 1995 and 2005. We calculated the effective
282 rainfall (ERF) as a difference between the rainfall (RF) and the actual evapotranspiration
283 (AET). We have no data for calculating AET, and we simplified the estimate using the
284 Penman potential evapotranspiration (PET)

285

$$\begin{cases} ERF = RF - PET, & \text{if } RF > PET \\ ERF = 0, & \text{if } RF \leq PET \end{cases} \quad (12)$$

286 Fig. 4c shows the Penman potential evapotranspiration estimated by Meteo France for the
 287 Orleans weather station (Lat.-47°59'24"N; Long.-1°46'36"E). Fig. 4d shows the effective
 288 rainfall (left axis) and the GWL (right axis).

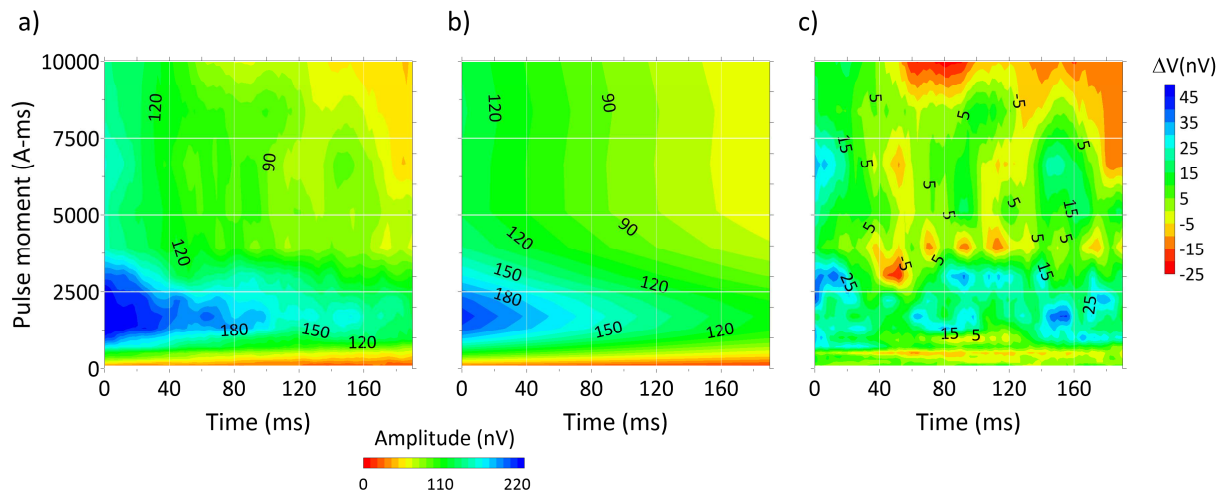


289

290 *Figure 4. a) The annual rainfall recorded in Villamblain between 1995 and 2006. b) The*
 291 *groundwater level variations. Gray rectangles show the time interval when the MRS*
 292 *monitoring was carried out. c) Daily records of the rainfall and the estimation of the Penman*
 293 *potential evapotranspiration during MRS monitoring. d) The cumulative effective rainfall (left*
 294 *axis) and the groundwater level (right axis).*

295

296 Fig. 5a shows measured amplitude of the MRS signal (color scale) versus time and pulse
 297 moment. Fig. 5b shows the theoretical signal computed after the MRS inverse model and Fig.
 298 5c shows the difference in-between.

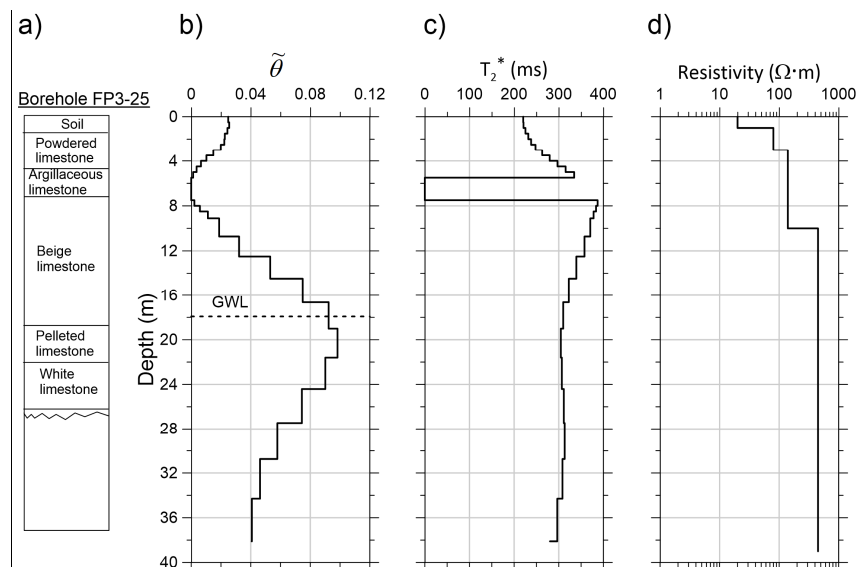


299

300 *Figure 5. a) Measured amplitude of the MRS signal (color scale) as a function of the pulse*
 301 *moment and time. b) Theoretical amplitude computed after the MRS inverse model. c) The*
 302 *difference between the measured and the theoretical amplitudes.*

303

304 Fig. 6 shows the results of a single MRS sounding (performed 13/08/1999). Figures 6b and 6c
 305 compare the water content and the relaxation time profiles with the lithological log of the
 306 borehole 03622X0119/FP3-25 (Fig. 6a). The distance between the borehole and the MRS
 307 loop located was 76 m. The resistivity profile was extracted from the ERT measurements.



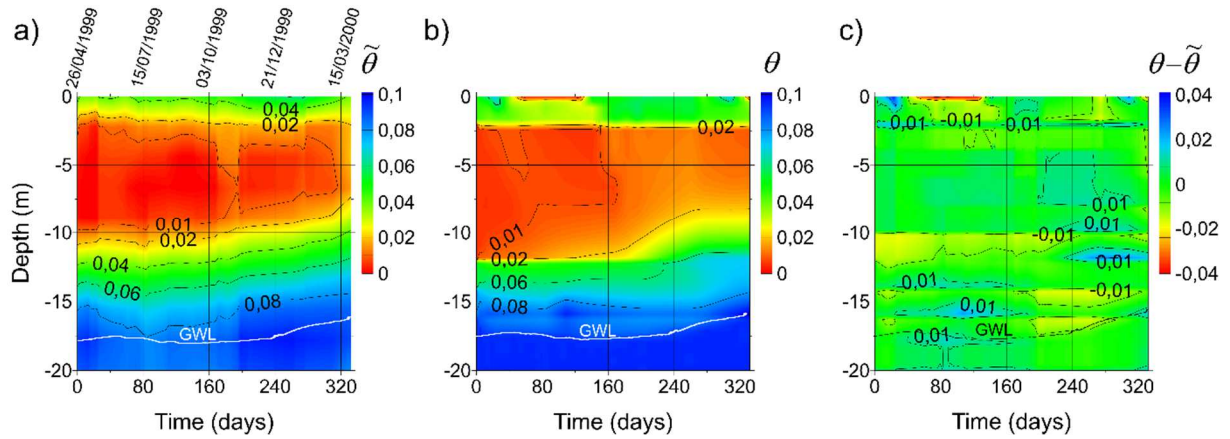
308

309 *Figure 6. a) The lithological log of the borehole 03622X0119/FP3-25 (Fig. 3). b,c) The water*
310 *content and the relaxation time T_2^* provided by the MRS inverse model. d) The electrical*
311 *resistivity profile.*

312

313 The MRS log (Fig. 6b) showed a smooth increase of the water content from the surface to the
314 GWL. Between 4 and 8 m, the MRS revealed a low water content, suggesting a clay layer
315 observed at this depth in the borehole. However, a long relaxation time and a high resistivity
316 (Figs. 6c and 6d) are typical for sand and do not confirm clay. Note that the observed low
317 water content may also correspond to an unsaturated fractured limestone that does not contain
318 much water. Because of the limited resolution, the MRS inversion did not identify the GWL
319 at 17 m. Below 25 m, decreasing water content corresponds to a lowering specific yield of the
320 saturated limestone. For this sounding, the average signal-to-noise ratio was high ($S/N = 9.56$)
321 and the theoretical signal fitted well the measured one.

322 The MRS time-lapse inversion showed two principal water storage zones between 0 and 2 m
323 and below 10 m (Fig. 7a). The water content in limestone ranged between 0.04 and 0.08.
324 These values are in good agreement with the specific yield in limestone reported between 0.03
325 and 0.13 (Schnebelen *et al.*, 1999). The MRS revealed less water between 2 and 10 m. This
326 observation may have two plausible explanations. The first one suggests a low-permeable clay
327 formation. The second explanation puts forward a permeable unsaturated material that does
328 not store much water when unsaturated. MRS alone cannot distinguish between these two
329 possibilities.



330

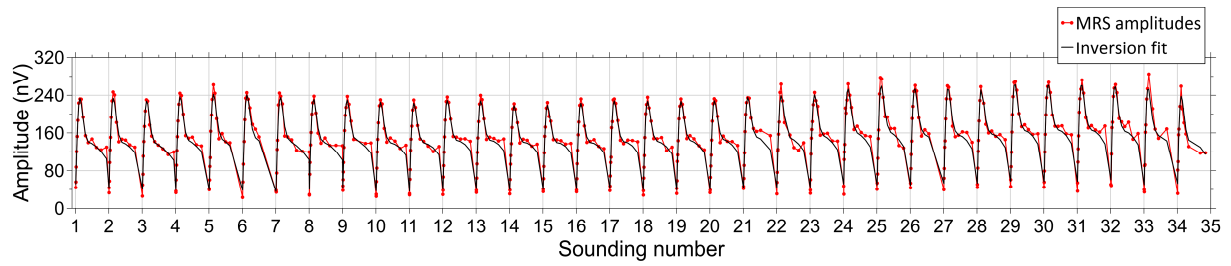
331 *Figure 7. a) The water content provided by the MRS inversion. b) The water content*
 332 *computed with the HYDRUS-1D program. c) The difference between these two images shows*
 333 *a good correspondence in-between. The maximum difference is less than 0.04, and the*
 334 *discrepancy is RMSE = 0.0079.*

335

336 In the water flow model, the MRS water content allowed us to select four layers with different
 337 hydraulic parameters: at depths of 0-2 m, 2-12 m, 12-16 m and 16-20 m. We had no data
 338 about the heterogeneity in the subsurface, and we used a simplified hydraulic model assuming
 339 a horizontal stratification. The last layer below 16 m was almost saturated and, for this layer,
 340 the MRS provided the θ_s . For the layers above the GWL, θ_s was a free parameter in
 341 inversion. Taking into account the same geological origin of the limestone, we assumed, as
 342 the first guess, θ_s of these layers equal to that measured with MRS in the saturated limestone.
 343 Then, the inversion routine adjusted θ_s . We had no data about the value of θ_r . However,
 344 considering that MRS cannot see water with the water content close to θ_r , we set
 345 $\theta_r = 0.001 \approx 0$ for all four layers. Note that both θ_s and θ_r measured with MRS at a large

346 scale were different compared to that measured on soil samples at a local scale. The MRS
347 sounding at time zero provided the initial water content for hydraulic modeling. We used the
348 Kosugi hydraulic property model without hysteresis. As recommended for many soils
349 (Mualem, 1976), we fixed the tortuosity parameter ($l=0.5$) in the conductivity function. Our
350 hydraulic model aimed to reproduce the unsaturated water flow observed with the MRS in
351 Villamblain and not to assess the hydraulic parameters of the subsurface. We assumed the
352 atmospheric boundary conditions with a surface layer as the upper limit and a variable
353 pressure head as the lower boundary condition. The meteorological data provided the daily
354 precipitation and the potential evapotranspiration. The groundwater level depended on
355 hydrological processes taking place at the watershed scale that is much larger compared to the
356 scale of our study and we considered the GWL level as an input variable in the hydraulic
357 model.

358 The MRS inversion provided the water content (Fig. 7a) consistent with that computed with
359 the hydraulic model (Fig. 7b). Fig. 7c shows the difference between these two images. The
360 root-mean-square error between the two images, each of them containing N values of the
361 water content, was $RMSE = \sqrt{N^{-1}(\theta - \tilde{\theta})^2} = 0.0079$. The amplitude of the MRS signal
362 computed after the time-lapse MRS inverse model fitted the measured MRS amplitude with
363 $RMSE=10.3$ nV and the theoretical signal computed after the water flow model with
364 $RMSE=10.9$ nV. The mean experimental noise was 14.2 nV. Fig. 8 shows the amplitude
365 versus pulse moment for all MRS soundings (red dots). A black line shows the amplitude
366 computed using the water content provided by the unsaturated water flow model.



367

368 *Figure 8. Measured amplitude of the MRS signal versus pulse moment for all soundings*
 369 *performed in Villamblain (red dots) and the theoretical amplitude computed after the water*
 370 *content provided by the unsaturated water flow model (black line). For each sounding, the*
 371 *pulse moment was normalized by the maximum pulse moment over all soundings.*

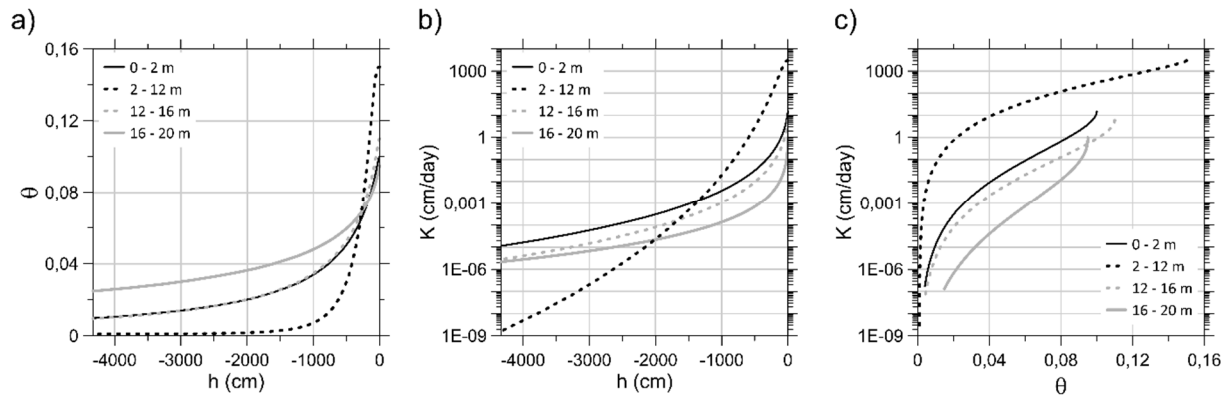
372

373 Table 1 and Fig. 9 present the soil hydraulic parameters in the water flow model.

Depth interval (m)	θ_r	θ_s	σ (1/cm)	n	K_s (cm/day)	l
0 - 2	0.001	0.1	500	1.6	15	0.5
2 - 12	0.001	0.15	250	0.8	3000	0.5
12 - 16	0.001	0.11	450	1.6	6	0.5
16 - 20	0.001	0.095	1000	2.2	1	0.5

374 *Table 1. The soil hydraulic parameters in Villamblain used in the unsaturated water flow*
 375 *model (the Kosugi hydraulic property model).*

376



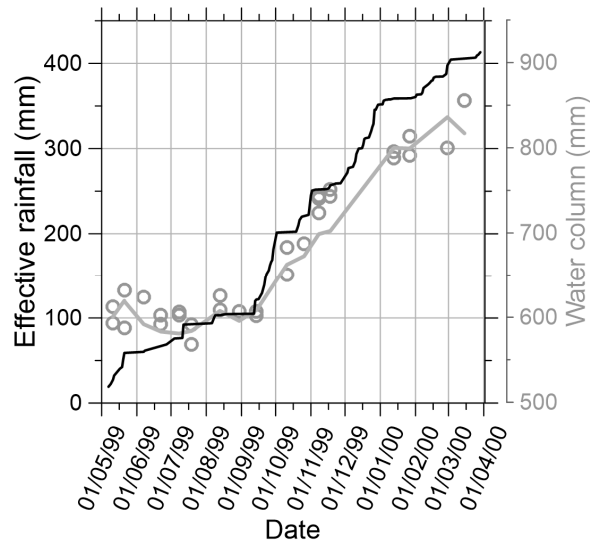
377

378 *Figure 9. The soil hydraulic functions of the four synthetic layers corresponding to the*
 379 *hydraulic parameters shown in Table 1.*

380

381 Fig. 9 shows the soil hydraulic functions of the four synthetic layers used in the water flow
 382 model. One layer exhibited hydraulic parameters typical for a permeable material (coarse sand
 383 or fractured limestone). This layer had a high hydraulic conductivity and low water content
 384 when not saturated. The borehole identified argillaceous limestone at this depth and we
 385 interpreted the layer between 2 and 12 m as fractured limestone containing some clay in the
 386 matrix. The MRS cannot see water in clay and showed no water in the limestone matrix.
 387 Fracturing rendered this formation permeable when saturated.

388 Fig. 10 shows the water column measured with the MRS in the depth interval between 0 and
 389 18 m (gray circles) and the water column provided by the water flow model (gray line). The
 390 black line shows the effective rainfall derived from the meteorological observations. These
 391 graphs show that in summer months (May-August), the water column diminished and water in
 392 the unsaturated zone contributed to the aquifers recharge. In September-December, the water
 393 column increased with the rate that followed the effective rainfall. Hence, the rainwater did
 394 not flow to the aquifer, but recharged the unsaturated zone. Since January, the water column
 395 was about constant and the effective rainfall recharged the aquifer.



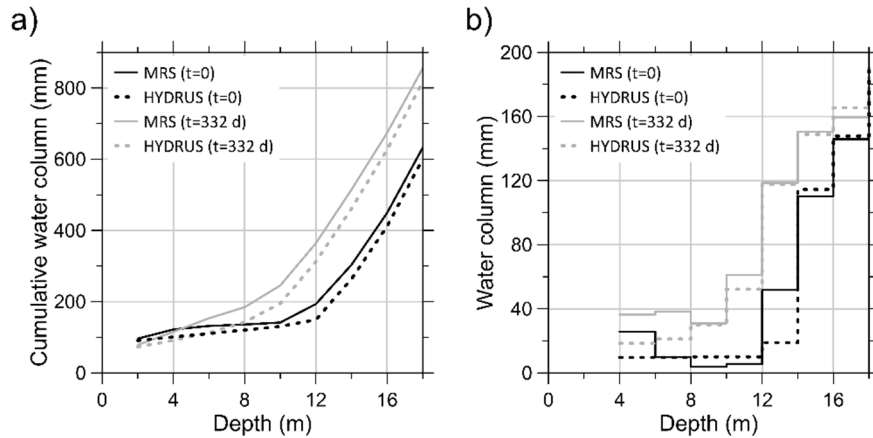
396

397 *Figure 10. The effective rainfall (black line, left vertical axis) versus time, and the water*
 398 *column in the depth interval between 0 and 18 m measured with MRS (gray circles, right*
 399 *vertical axis). The gray line shows the water column provided by the water flow modeling.*

400

401 Fig. 10 shows the cumulative effective rainfall (totally 413 mm). It was shared between the
 402 increase of the water column in the unsaturated zone (211 mm) and the actual
 403 evapotranspiration plus the aquifer recharge (202 mm). We had no data for estimating the
 404 AET, and hence we cannot quantify the aquifer recharge. However, taking into account the
 405 mean annual recharge of the Beauce aquifer (110 mm) (*Schnebelen et al., 1999*), we
 406 considered that our results were in a reasonable agreement with the existing data. Fig. 10
 407 shows that the water column increased with the rate that followed the cumulative effective
 408 rainfall. For comparison, the rise of GWL (Fig. 4d) showed a three-month delay relative to the
 409 effective rainfall. These observations confirm that MRS quantified water in the unsaturated
 410 zone and not in the aquifer.

411 Fig. 11a shows the cumulative water column versus depth at the very beginning and the very
 412 end of the monitoring time. The derivative of the cumulative water volume suggested the
 413 principal water storage zone between 10 and 16 m (Fig. 11b).



414

415 *Figure 11. The cumulative water column in the unsaturated zone versus depth measured with*
 416 *the MRS (solid lines) and that computed with the water flow model (dashed lines). We show*
 417 *the results corresponding to the first (t=0) and the last (t=332 d) days of monitoring. a) The*
 418 *cumulative water column. b) The water column versus depth computed with the step of 2 m.*

419

420 DISCUSSION

421 Our results confirmed the possibility of developing an unsaturated water flow model using
 422 MRS time-lapse measurements. We did not aim to quantify the hydraulic parameters of the
 423 subsurface, but to reproduce the water content profile observed with MRS. The use of more
 424 geological, hydrological and meteorological data opens the way for improving the accuracy of
 425 the model.

426 As with any other method, MRS has specific features to consider for practical applications.

- 427 • Soils and rocks of different geological origins may have different values of the
428 magnetic susceptibility and of the surface relaxivity rate. It renders the error of the
429 water content measurements with MRS ($\Delta\theta$) site dependent.
- 430 • The insufficient accuracy of MRS measurements does not allow measuring the water
431 content close to θ_r .
- 432 • Soils and rocks containing paramagnetic inclusions disturb the homogeneity of the
433 Earth's magnetic field. It may bias the water content measurements with the MRS
434 (*Legchenko et al.*, 2010; *Costable et al.*, 2018). In the unsaturated zone, this effect is
435 stronger than in an aquifer and the MRS can monitor the water content in the
436 unsaturated zone only in materials with a low magnetic susceptibility ($<10^{-5}$ SIU). For
437 example, in limestone or chalk.
- 438 • MRS provides the water content averaged over a large area. It limits the lateral
439 resolution of the method. Application of 2-D (*Hertrich et al.*, 2007) and 3-D
440 (*Legchenko et al.*, 2011) tomographic measurements can improve the lateral
441 resolution. But the tomographic measurements are more time and labor consuming.
442 *Jiang et al.* (2015) proposed a compromise between the resolution and the measuring
443 time. It comprises the use of one large transmitting loop and a few smaller receiving
444 loops.
- 445 • One standard MRS sounding requires at least two to three hours of measuring. We
446 assumed the water content in the subsurface to be invariable during this time. A long
447 measuring time imposes a limitation on the rapidity of investigated hydrological
448 processes. After our experience, the monitoring rate of one sounding per day is close
449 to the limit of the method. Note that this limitation is not a physical but a technical
450 one.

451 **CONCLUSIONS**

452 Time lapse MRS measurements make it possible to quantify water content variations in the
453 unsaturated media composed of materials with low magnetic susceptibility (chalk, limestone).
454 It does not exist any other method that provides non-invasive measurements of the water
455 content down to a few tens of meters. The MRS water content profile can contribute to
456 unsaturated water flow modeling. However, one should keep in mind the particularity of the
457 MRS measurements. The MRS averages the water content over a large volume defined by the
458 loop size. The accuracy of the MRS results is site dependent. One sounding requires a few
459 hours of measuring, which limits the MRS capacity to investigate rapid processes. It does not
460 exist other methods that would allow a direct verification of the MRS results. It renders the
461 MRS accuracy in terms of water content difficult to estimate. In this paper, we showed the
462 possibility of performing water flow modeling using Richards equations. However, the MRS
463 can contribute to any other hydraulic model.

464 During our study, we approximated the unsaturated zone in Villamblain by a horizontally
465 stratified subsurface. Despite simplicity, the model allowed us to reproduce the water content
466 variations observed with MRS. We are looking forward to verifying our approach by
467 performing a new monitoring at the same place. Such a monitoring will provide the water
468 content profile with a 20-years shift relative to 2000. Then, we will use the parameters of the
469 model established in 1999-2000 for predicting the water content observed in 2020-2021.

470 **ACKNOWLEDGEMENTS**

471 The authors carried out this study in the laboratory IGE - IRD (Grenoble) with the support of
472 the BRGM and the IRD research programs. We acknowledge financial support from Labex
473 OSUG@2020 (Investissements d'avenir – ANR10 LABX56) and the French National
474 Program (ANR) "Investment for Future - Excellency Equipment" project EQUIPEX CRITEX

475 (grant # ANR-11-EQPX-0011). We are thankful to Dr. Maciek Lubczynski and two
476 anonymous reviewers for their critical comments that helped us to improve presentation of
477 our results.

478 **References**

479 Andersen, K. R., L. Wan, D. Grombacher, T. Lin, and E. Auken, 2018, Studies of parameter
480 correlations in surface NMR using the Markov chain Monte Carlo method, *Near Surf.*
481 *Geophys.*, 16, 206-217, doi.org/10.3997/1873-0604.2017064.

482 Aster, R. C., B. Borchers, and C. H. Thurber, 2012, Parameter Estimation and Inverse
483 Problems 2nd edition, *Academic Press*, 376 pp., eBook ISBN: 9780123850492.

484 Baroncini-Turricchia, G., A. P. Francés, M. W. Lubczynski, J. Martínez-Fernández, and J.
485 Roy, 2014, Integrating MRS data with hydrologic model - Carrizal Catchment, Spain, *Near*
486 *Surf. Geophys.*, 12, 2, 255-269, doi: 10.3997/1873-0604.2014003.

487 Behroozmand, A., E. Auken, G. Fiandaca, and A. V. Christiansen, 2012, Improvement in
488 MRS parameter estimation by joint and laterally constrained inversion of MRS and TEM
489 data, *Geophysics*, 77, WB191–WB200, doi:10.1190/GEO2011-0404.1.

490 Behroozmand, A. A., K. Keating, E. Auken, 2015, A review of the principles and applications
491 of the NMR technique for near-surface characterization, *Surv. Geophys.* 36, 1, 27-85,
492 doi:10.1007/s10712-014-9304-0.

493 Binley, A., S. S. Hubbard, J. A. Huisman, A. Revil, D. A. Robinson, K. Singha, and L. D.
494 Slater, 2015, The emergence of hydrogeophysics for improved understanding of subsurface
495 processes over multiple scales, *Water Resour. Res.*, 51, 3837-3866,
496 doi:10.1002/2015WR017016.

- 497 Boucher, M., A. Legchenko, J. M. Baltassat, F. Mathieu, 2003, Étude des variations
498 temporelles du signal RMP en comparaison avec le niveau piézométrique sur le site de
499 Villamblain (Loiret), *BRGM*, BRGM/RP-52310-FR, 43 p., 21 fig., 3 tabl., 2 ann. (volume
500 séparé).
- 501 Boucher, M., G. Favreau, M. Descloitres, J-M. Vouillamoz, S. Massuel, Y. Nazoumou, B.
502 Cappelaere, A. Legchenko, 2009, Contribution of geophysical surveys to groundwater
503 modelling of a porous aquifer in semiarid Niger: An overview, *C. R. Geoscience*, 341, 10-
504 11, 800-809, doi:10.1016/j.crte.2009.07.008.
- 505 Boucher, M., G. Favreau, Y. Nazoumou, B. Cappelaere, S. Massuel, A. Legchenko, 2012,
506 Constraining Groundwater Modeling with Magnetic Resonance Soundings, *Ground Water*,
507 5, 5, 775-784, doi:10.1111/j.1745-6584.2011.00891.x.
- 508 Bourenane, H., D. King, R. Le Parco, M. Isambert, A. Tabbagh, 1998, Three-dimensional
509 analysis of soils and surface materials by electrical resistivity survey, *Eur. J. Environ. Eng.*
510 *Geophys.* 3, 5–23.
- 511 Bruand, A., G. Creuzot, P. Quéting, R. Darthout, L. Raison, P. Courtemanche, et H. Gaillard,
512 1997, Variabilité de la recharge de la nappe de Beauce – Rôle de l’irrigation et des
513 caractéristiques du sol, *Etude et Gestion des sols*, Association française pour l’étude des
514 *sols*, 4, 229-245, <hal-00089036>.
- 515 Campbell, G. S., 1974, A simple method for determining unsaturated conductivity from
516 moisture retention data, *Soil Sci.*, 117, 6, 311-317.
- 517 Camporese, M., G. Cassiani, R. Deiana, and P. Salandin, 2012, Assessment of local hydraulic
518 properties from electrical resistivity tomography monitoring of a three-dimensional

519 synthetic tracer test experiment, *Water Resour. Res.*, 47, W12508,
520 doi:10.1029/2011WR010528.

521 Carrière, S. D, K. Chalikakis, G. Sénéchal, C. Danquigny, C. Emblanch, 2013, Combining
522 Electrical Resistivity Tomography and Ground Penetrating Radar to study geological
523 structuring of karst Unsaturated Zone, *J. Appl. Geophys.*, 94, 31-41,
524 doi:10.1016/j.jappgeo.2013.03.014.

525 Carrière, S. D., K. Chalikakis, C. Danquigny, H. Davi, N. Mazzilli, C. Ollivier, C. Emblanch,
526 2016, The role of porous matrix in water flow regulation within a karst unsaturated zone:
527 an integrated hydrogeophysical approach, *Hydrogeol. J.*, 24, 1905-1918,
528 doi:10.1007/s10040-016-1425-8

529 Chalikakis, K., M. R Nielsen, and A. Legchenko, 2008, MRS applicability for a study of
530 glacial sedimentary aquifers in Central Jutland, Denmark, *J. Appl. Geophys.*, 66, 3-4, 176-
531 187, doi:10.1016/j.jappgeo.2007.11.005.

532 Chaudhuri, A., M. Sekhar, M. Descloitres, Y. Godderis, L. Ruiz, J. J. Braun, 2013,
533 Constraining complex aquifer geometry with geophysics (2-D ERT and MRS
534 measurements) for stochastic modelling of groundwater flow, *J. Appl. Geophys.*, 98, 288-
535 297, doi:10.1016/j.jappgeo.2013.09.005.

536 Chéry, P., O. Lavialle, H. Bourennane, D. King, A. Bruand, 1999, Variabilité verticale de la
537 composition granulométrique des limons de Petite Beauce (France), *Etude et Gestion des*
538 *Sols, Association française pour l'étude des sols*, 6, 185-196, <hal-00089054>.

539 Chevalier, A., A. Legchenko, J-F Girard, M., Descloitres, 2014, 3D Monte Carlo inversion of
540 Magnetic Resonance measurements, *Geophys. J. Int.*, 198, 216-228,
541 doi:10.1093/gji/ggu091.

542 Comte, J-C., U. Ofterdinger, A. Legchenko, J. Caulfield, R. Cassidy, and J. A. Mézquita
543 González, 2018, Catchment-scale heterogeneity of flow and storage properties in a
544 weathered/fractured hard rock aquifer from resistivity and magnetic resonance surveys:
545 implications for groundwater flow paths and the distribution of residence times, *Geol. Soc.*
546 *London*, Special Publications, 479, 10 May 2018, doi:10.1144/SP479.11.

547 Costabel, S., and U. Yaramanci, 2011, Relative hydraulic conductivity in the vadose zone
548 from magnetic resonance sounding - Brooks-Corey parameterization of the capillary
549 fringe, *Geophysics*, 76, 3, B1–B11, doi:10.1190/1.3552688.

550 Costabel, S., C. Weidner, M. Müller-Petke, and G. Houben (2018), Hydraulic characterisation
551 of iron-oxide-coated sand and gravel based on nuclear magnetic resonance relaxation mode
552 analyses, *Hydrol. Earth Syst. Sci.*, 22, 1713-1729, doi:10.5194/hess-22-1713-2018.

553 Creuzot, G., F. Brunson, R. Grave, 1997, Variations piézométriques de la nappe des calcaires
554 de Beauce 1996, *Rapport DIREN Centre*, SEMA, 86 p.

555 Descloitres, M., L. Ruiz, M. Sekhar, A. Legchenko, J-J. Braun, M. S. Mohan Kumar, S.
556 Subramanian, 2008, Characterization of seasonal local recharge using Electrical Resistivity
557 Tomography and Magnetic Resonance Sounding, *Hydrol. Processes*, 22, 3, 384-394,
558 doi:10.1002/hyp.6608.

559 Desprez, N., et C. Megnien, 1975, Atlas hydrogéologique de la Beauce, *BRGM*, Service
560 géologique régional du bassin de Paris, Orleans, 112 p.

561 Deumier, J. M., A. Bouthier, B. Lacroix, F. Golaz, 2001, Raisonner l'arrêt de l'irrigation sur le
562 maïs, *Perspectives Agricoles*, 270, 70-75.

563 Dunn, K. J., D. J. Bergman and G. A. Latorraca, 2002, Nuclear Magnetic Resonance
564 Petrophysical and Logging Applications, *Elsevier Science Ltd, UK*.

565 Durner, W., 1994, Hydraulic conductivity estimation for soils with heterogeneous pore
566 structure, *Water Resour. Res.*, 30, 2, 211–223, doi10.1029/93WR02676.

567 Falzone, S., and K. Keating, 2016, Algorithms for removing surface water signals from
568 surface nuclear magnetic resonance infiltration surveys, *Geophysics*, 81, 4, WB97–
569 WB107. doi: 10.1190/geo2015-0386.1.

570 Favreau, G., B. Cappelaere, S. Massuel, M. Leblanc, M. Boucher, N. Boulain, C. Leduc,
571 2009, Land clearing, climate variability and water resources increase in semiarid southwest
572 Niger: a review, *Water Resour. Res.*, 45, W00A16, doi:10.1029/2007WR006785.

573 Garambois, S., A. Legchenko, C. Vincent, E. Thibert, 2016, Ground-penetrating radar and
574 surface nuclear magnetic resonance monitoring of an englacial water-filled cavity in the
575 polythermal glacier of Tête Rousse, *Geophysics*, 81, 1, WA131–WA146,
576 doi:10.1190/GEO2015-0125.1.

577 Grombacher, D., L. Liu, J. J. Larsen, E. Auken, 2018, Practical considerations for small
578 receive coils in surface NMR, *J. Appl. Geophys.*, 154, 81-92, doi:
579 10.1016/j.jappgeo.2018.04.005.

580 Guillen, A., and A. Legchenko, 2002a, Inversion of Surface Nuclear Magnetic Resonance
581 data by an adapted Monte-Carlo method applied to water resource characterization, *J.*
582 *Appl. Geophys.*, 50, 193-205, doi:10.1016/S0926-9851(02)00139-8.

583 Guillen, A., and A. Legchenko, 2002b, Application of linear programming techniques to the
584 inversion of proton magnetic resonance measurements for water prospecting from the
585 surface, *J. Appl. Geophys.*, 50, 149-162, doi:10.1016/S0926-9851(02)00136-2.

586 Herckenrath, D., E. Auken, L. Christiansen, A. A. Behroozmand, P. Bauer-Gottwein, 2012,
587 Coupled hydrogeophysical inversion using time-lapse magnetic resonance sounding and
588 time-lapse gravity data for hydraulic aquifer testing: Will it work in practice?, *Water*
589 *Resour. Res.*, 48, W01539, doi:10.1029/2011WR010411.

590 Hertrich, M., M. Braun, T. Günther, A. G. Green, U. Yaramanci, 2007, Surface nuclear
591 magnetic resonance tomography, *IEEE Trans. Geosci. Remote Sens.*, 45, 11, 3752–3759,
592 doi:10.1109/TGRS.2007.903829.

593 Hertrich, M., 2008, Imaging of groundwater with nuclear magnetic resonance, *Prog. Nucl.*
594 *Magn. Reson. Spectrosc.*, 53, 227–248, doi:10.1016/j.pnmrs.2008.01.002.

595 Høyer, A-S., F. Jørgensen, N. Foged, X. He, A. V. Christiansen, 2011, Three-dimensional
596 geological modelling of AEM resistivity data - A comparison of three methods, *J. Appl.*
597 *Geophys.*, 115, 65-78, doi:10.1016/j.jappgeo.2015.02.005.

598 Ikard, S., and E. Pease, 2019, Preferential groundwater seepage in karst terrane inferred from
599 geoelectric measurements, *Near Surf. Geophys.*, 2019, 17, 43-53, doi:10.1002/nsg.12023.

600 Irons, T. P., and Y. Li, 2014, Pulse and Fourier transform surface nuclear magnetic resonance:
601 comprehensive modelling and inversion incorporating complex data and static dephasing
602 dynamics, *Geophys. J. Int.*, 199(3), 1372-1394, doi:10.1093/gji/ggu323.

603 Jajarmizadeh, M., Harun, S., and Salarpour, M., 2012, A Review on Theoretical
604 Consideration and Types of Models in Hydrology, *Environ. Sci. Technol.*, 5, 5, 249-261, doi:
605 10.3923/jest.2012.249.261.

606 Jiang, C., M. Müller-Petke, J. Lin, and U. Yaramanci, 2015, Magnetic resonance tomography
607 using elongated transmitter and in-loop receiver arrays for time-efficient 2-D imaging of
608 subsurface aquifer structures, *Geophys. J. Int.*, 200, 824–836, doi:10.1093/gji/ggu434.

609 Jodry, C., A. Isch, C. Aldana, M. Azaroual, M. Klintzing, 2018, Geoelectrical imaging of the
610 vadoze zone of an observation site of the Beauce aquifer at Villamblain, 11 Colloque
611 GEOFCAN, 20 et 21 novembre 2018, Antony, France. Jouen, T., R. Clément, H. Henine,
612 C. Chaumont, B. Vincent, J. Tournebize, 2018, Evaluation and localization of an artificial
613 drainage network by 3D time-lapse electrical resistivity tomography, *Environ Sci Pollut*
614 *Res Int.*, 25(24), 23502-23514, doi:10.1007/s11356-016-7366-x.

615 Kemna, A., J. Vanderborcht, B. Kulesa, and H. Vereecken, 2002, Imaging and
616 characterisation of subsurface solute transport using electrical resistivity tomography
617 (ERT) and equivalent transport models, *J. Hydrol.*, 267, 3–4, 125–146, doi:10.1016/S0022-
618 1694(02)00145-2.

619 Kenyon, W. E., 1997, Petrophysical Principles of Applications of NMR Logging, *The Log*
620 *Analyst*, 21-43.

621 Kosugi, K., 1994, Three-parameter lognormal distribution model for soil water retention,
622 *Water Resour. Res.*, 30, 4, 891-901, doi:10.1029/93WR02931.

623 Kosugi, K., 1996, Lognormal distribution model for unsaturated soil hydraulic properties,
624 *Water Resour. Res.*, 32, 9, 2697-2703, doi:10.1029/96WR01776.

625 Kowalski, M. B., S. Finsterle, and Y. Rubin, 2004, Estimating slow parameter distributions
626 using ground-penetrating radar and hydrological measurements during transient flow in the
627 vadose zone, *Adv. Water Resour.*, 27, 583-599, doi:10.1016/j.advwatres.2004.03.003.

628 Legchenko, A. V., A. Beauce, A. Guillen, P. Valla, and J. Bernard, 1997, Natural variations in
629 the magnetic resonance signal used in PMR groundwater prospecting from the surface,
630 *European J. Environ. Eng. Geoph.*, 2, 173-190.

631 Legchenko, A. V., and O. A. Shushakov, 1998, Inversion of surface NMR data, *Geophysics*,
632 63, 1, 75-84, doi:10.1190/1.1444329.

633 Legchenko, A., and P. Valla, 2002, A review of the basic principles for proton magnetic
634 resonance sounding measurements, *J. Appl. Geophys.*, 50, 3-19, doi:10.1016/S0926-
635 9851(02)00127-1.

636 Legchenko, A., J-M. Baltassat, A. Beauce, J. Bernard, 2002, Nuclear magnetic resonance as a
637 geophysical tool for hydrogeologists, *J. Appl. Geophys.* 50, 21-46, doi:10.1016/S0926-
638 9851(02)00128-3.

639 Legchenko, A., J-M. Baltassat, A. Bobachev, C. Martin, H. Robin, J.-M. Vouillamoz, 2004,
640 Magnetic resonance sounding applied to aquifer characterization, *Ground Water*, 42, 3,
641 363-373, doi:10.1111/j.1745-6584.2004.tb02684.x.

642 Legchenko, A., M. Ezersky, C. Camerlink, A. Al-Zoubi, K. Chalikakis, and J-F. Girard, 2008,
643 Locating water-filled karst caverns and estimating their volume using magnetic resonance
644 soundings, *Geophysics*, 73, 5, 51-61, doi:10.1190/1.2958007.

645 Legchenko, A., J-M. Vouillamoz, and J. Roy, 2010, Application of the magnetic resonance
646 sounding method to the investigation of aquifers in the presence of magnetic materials,
647 *Geophysics*, 75 (6), L91–L100, doi:10.1190/1.3494596.

648 Legchenko, A., M. Descloitres, C. Vincent, H. Guyard, S. Garambois, K. Chalikakis, and M.
649 Ezersky, 2011, Three-dimensional magnetic resonance imaging for groundwater, *New J.*
650 *Phys.*, 13, 025022, doi:10.1088/1367-2630/13/2/025022.

651 Legchenko, A., 2013, Magnetic resonance imaging for groundwater, Wiley-ISTE, 158 pp.,
652 Online ISBN:9781118649459, doi:10.1002/9781118649459.

653 Legchenko A., and G. Pierrat, 2014, Glimpse into the design of MRS instrument, *Near Surf.*
654 *Geophys.*, 12, 297-308, doi:10.3997/1873-0604.2014006.

655 Legchenko, A., C. Vincent, J-M. Baltassat, J-F. Girard, E. Thibert, O. Gagliardini, M.,
656 Descloitres, A. Gilbert, S. Garambois, A. Chevalier, and H. Guyard, 2014, Monitoring
657 water accumulation in a glacier using magnetic resonance imaging, *Cryosphere*, 8, 155-
658 166, doi:10.5194/tc-8-155-2014.

659 Legchenko A., J-C. Comte, U. Ofterdinger, J-M. Vouillamoz, F. M. A. Lawson, and J. Walsh,
660 2017, Joint use of singular value decomposition and Monte-Carlo simulation for estimating
661 uncertainty in surface NMR inversion, *J. Appl. Geophys.*, 144, 28-36,
662 doi:10.1016/j.jappgeo.2017.06.010.

663 Lepiller, M., 2006, Le Val d'Orléans. In: Aquifères et eaux souterraines en France, tome 1, J.-
664 C. Roux (éd.), *BRGM Éditions*.

665 Lubczynski, M., and J. Roy, 2003, Hydrogeological interpretation and potential of the new
666 magnetic resonance sounding (MRS) method, *J. Hydrol.*, 283, 19–40, doi:10.1016/S0022-
667 1694(03)00170-7.

668 Lubczynski, M., and J. Roy, 2004, Magnetic resonance sounding: new method for ground
669 water assessment, *Ground Water*, 42, 291-303, doi:10.1111/j.1745-6584.2004.tb02675.x.

670 Lubczynski, M., and J. Gurwin, 2005, Integration of various data sources for transient
671 groundwater modeling with spatio-temporally variable fluxes - Sardon study case, Spain. *J.*
672 *Hydrol.* 306, 71–96, doi:10.1016/j.jhydrol.2004.08.038.

673 Madi, R., G. H. de Rooij, H. Mielenz, and J. Mai,(2018, Parametric soil water retention
674 models: A critical evaluation of expressions for the full moisture range, *Hydrol. Earth Syst.*
675 *Sci.*, 22, 1193-1219, doi:10.5194/hess-22-1193-2018.

676 Marquardt, D. W., 1963, An algorithm for least-squares estimation of nonlinear parameters, *J.*
677 *Soc. Indust. Appl. Math.*,11, 2, 431-441, doi: 10.1137/0111030.

678 Michot, D., Y. Benderitter, A. Dorigny, B. Nicoullaud, D. King, and A. Tabbagh, 2003,
679 Spatial and temporal monitoring of soil water content with an irrigated corn crop cover
680 using surface electrical resistivity tomography, *Water Resour. Res.*, 39(5), 1138,
681 doi:10.1029/2002WR001581.

682 Mohnke, O, and U. Yaramanci, 2002, Smooth and block inversion of surface NMR
683 amplitudes and decay times using simulated annealing, *J. Appl. Geophys.*, 50, 163-177,
684 doi:10.1016/S0926-9851(02) 00137-4.

685 Mohnke, O., 2014, Jointly deriving NMR surface relaxivity and pore size distributions by
686 NMR relaxation experiments on partially desaturated rocks, *Water Resour. Res.*, 50, 5309–
687 5321, doi:10.1002/2014WR015282.

688 Mualem, Y., 1976, A new model for predicting the hydraulic conductivity of unsaturated
689 porous media, *Water Resour. Res.*, 12, 3, 513-522, doi:10.1029/WR012i003p00513.

690 Müller-Petke, M., U. Yaramanci, 2008, Resolution studies for Magnetic Resonance Sounding
691 (MRS) using the singular value decomposition, *J. Appl. Geophys.*, 66, 165-175,
692 doi:10.1016/j.jappgeo.2007.11.004.

693 Müller-Petke, M., U. Yaramanci, 2010, QT inversion - Comprehensive use of the complete
694 surface NMR data set, *Geophysics*; 75 (4): WA199–WA209, doi: 10.1190/1.3471523.

695 Müller-Petke, M., T. Hiller, R. Herrmann, U. Yaramanci, 2011, Reliability and limitations of
696 surface NMR assessed by comparison to borehole NMR, *Near Surf. Geophys.*, 9, 123-134,
697 doi:10.3997/1873-0604.2010066.

698 Nielsen M. R., T. F. Hagensen, K., Chalikakis, and A. Legchenko, 2011, Comparison of
699 transmissivities from MRS and pumping tests in Denmark, *Near Surf. Geophys.*, 9, 211-
700 223, doi:10.3997/1873-0604.2010071.

701 Park, C-H., A. Behrendt, E. LeDrew, and V. Wulfmeyer, 2017, New Approach for
702 Calculating the Effective Dielectric Constant of the Moist Soil for Microwaves, *Remote*
703 *Sens.*, 2017, 9, 32; doi:10.3390/rs9070732.

704 Parsekian, A. D., D. Grombacher, 2015, Uncertainty estimates for surface nuclear magnetic
705 resonance water content and relaxation time profiles from bootstrap statistics, *J. Appl.*
706 *Geophys.*, 119, 61–70, doi:10.1016/j.jappgeo.2015.05.005.

707 Poulsen, T. G., P. Moldrup, B.V. Iversen, O. H. Jacobsen, 2002, Three-region Campbell
708 model for unsaturated hydraulic conductivity in undisturbed soils, *Soil Sci. Soc. Am. J.*, 66,
709 744-752, doi:10.2136/sssaj2002.0744.

710 Power, C., P. Tsourlos, M. Ramasamy, A. Nivorlis, M. Mkandawire, 2018, Combined DC
711 resistivity and induced polarization (DC-IP) for mapping the internal composition of a
712 mine waste rock pile in Nova Scotia, Canada, *J. Appl. Geophys.*, 150, 40-51,
713 doi:10.1016/j.jappgeo.2018.01.009.

714 Roy, J., and M. Lubczynski, 2003, The magnetic resonance sounding technique and its use for
715 groundwater investigations, *Hydrogeol. J.*, 11, 455-465, doi:10.1007/s10040-003-0254-8.

716 Roy, J., and M. W. Lubczynski, 2005, MRS multi-exponential decay analysis: aquifer pore
717 size distribution and Vadose zone characterization, *Near Surf. Geophys.*, 3, 4, 287-298,
718 doi:10.3997/1873-0604.2005024.

719 Rubin, Y., and S. Hubbard, 2006, Hydrogeophysics, *Springer*, 523 p.

720 Saito, H., S. Kuroda, T. Iwasaki, H. Fujimaki, N. Nagai, J. Sala, 2018, Tracking Infiltration
721 Front Depth Using Time-lapse Multi-offset Gathers Collected with Array Antenna Ground
722 Penetrating Radar, *J. Vis. Exp.*, 135, e56847, doi:10.3791/56847.

723 Schaap, M. G., F. J. Leij, and M. Th. van Genuchten, 2001, Rosetta: A computer program for
724 estimating soil hydraulic parameters with hierarchical pedotransfer functions, *J. Hydrol.*,
725 251, 163-176, doi:10.1016/S0022-1694(01)00466-8.

726 Schirov, M., A. Legchenko, and G. Creer, 1991, New direct non-invasive ground water
727 detection technology for Australia, *Exploration Geophysics*, 22, 333-338.

728 Schnebelen, N, E. Ledoux, A. Bruand, G. Creuzot, 1999, Stratification hydrogéochimique et
729 écoulements verticaux dans l'aquifère des calcaires de Beauce (France) : un système
730 anthropisé à forte variabilité spatiale et temporelle, *Comptes rendus hebd. séances acad.*
731 *sci. Paris*, 329, 421-428, doi:10.1016/S1251-8050(00)80066-X.

732 Seevers, D. O., 1966, A nuclear magnetic method for determining the permeability of
733 sandstones, paper L, in *Annual Logging Symposium Transactions: Society of Professional*
734 *Well Log Analysts*.

735 Šimůnek, J., M. Šejna, H. Saito, M. Sakai, and M. Th. van Genuchten, 2008a, The HYDRUS-
736 1D software package for simulating the one-dimensional movement of water, heat, and
737 multiple solutes in variably-saturated media, Version 4.0, Hydrus Series 3, Department of
738 Environmental Sciences, *University of California Riverside*, Riverside, CA, USA, 2008.

739 Šimůnek, J., M. Th. van Genuchten, and M. Šejna, 2008b, Development and applications of
740 the HYDRUS and STANMOD software packages, and related codes, *Vadose Zone*
741 *Journal*, Special Issue "Vadose Zone Modeling", 7, 2, 587-600,
742 doi:10.2136/VZJ2007.0077.

743 Sood, A., and V. Smakhtin, 2015, Global hydrological models: a review, *Hydrological*
744 *Sciences Journal*, 60, 4, 549-565, doi: 10.1080/02626667.2014.950580.

745 Tikhonov, A., and Arsenin, V. 1977, Solution of ill-posed problems, *John Wiley & Sons,*
746 *Inc.* Valois, R., J-M. Vouillamoz, L. Arnout, 2018, Mapping groundwater reserves in
747 northwestern Cambodia with the combined use of data from lithologs and time-domain-
748 electromagnetic and magnetic-resonance soundings, *Hydrogeol. J.*, 26, 4, 1187–1200,
749 doi:10.1007/s10040-018-1726-1.

750 van Genuchten, M. T., 1980, A closed-form equation for predicting the hydraulic conductivity
751 of un-saturated soils, *Soil Sci. Soc. Am. J.*, 44, 892–898,
752 doi:10.2136/sssaj1980.03615995004400050002x.

753 Vereecken, H., J. Huisman, F. H. Hendricks, N. Bruggemann, H. Bogaen, S. Kollet, M.
754 Javaux, J. Van Der Kruk, and J. Vanderborght, 2015, Soil hydrology: Recent
755 methodological advances, challenges, and perspectives, *Water Resour. Res.*, 51, 2616-
756 2633, doi:10.1002/2014WR016852.

757 Vilhelmsen, T. N., A. A. Behroozmand, S. Christensen, and T. H. Nielsen, 2014, Joint
758 inversion of aquifer test, MRS, and TEM data, *Water Resour. Res.*, 50, 3956–3975,
759 doi:10.1002/2013WR014679.

760 Vouillamoz, J-M., M. Descloitres, G. Toe, A. Legchenko, 2005) Characterization of
761 crystalline basement aquifers with MRS: a case study in Burkina Faso, *Near Surf.*
762 *Geophys.*, 3, 3, 205-213, doi:10.3997/1873-0604.2005015.

763 Vouillamoz, J-M., G. Favreau, S. Massuel, M. Boucher, Y. Nazoumou, A. Legchenko, 2008,
764 Contribution of magnetic resonance sounding to aquifer characterization and recharge
765 estimate in semiarid Niger, *J. Appl. Geophys.*, 64, 3-4, 99-108,
766 doi:10.1016/j.jappgeo.2007.12.006.

767 Vouillamoz, J-M., A. Legchenko, and L. Nandagiri, 2011, Characterizing aquifers when using
768 magnetic resonance sounding in a heterogeneous geomagnetic field, *Near Surf. Geophys.*,
769 9, 135-144, doi:10.3997/1873-0604.2010053.

770 Vouillamoz, J-M., J. Hoareau, M. Grammare, D. Caron, L. Nandagiri, A. Legchenko, 2012,
771 Quantifying aquifer properties and freshwater resource in coastal barriers: a

772 hydrogeophysical approach applied at Sasihithlu (Karnataka state, India), *Hydrol. Earth*
773 *Syst. Sci.*, 16, 4387–4400, doi:10.5194/hess-16-4387-2012.

774 Vouillamoz, J. M., P. Sophoeun, O. Bruyere, and L. Arnout, 2013, Estimating storage
775 properties of aquifer with magnetic resonance sounding: a field verification in northern
776 Cambodia of the gravitational water apparent cutoff time concept, *Near Surf. Geophys.*, 12,
777 2, 211-2018, doi:10.3997/1873-0604.2013038.

778 Walsh, D. O., 2008, Multi-channel surface NMR instrumentation and software for 1D/2D
779 groundwater investigations, *J. Appl. Geophys.*, 66, 140–150,
780 doi:10.1016/j.jappgeo.2008.03.006. Walsh, D. O., E. D. Grunewald, P. Turner, A. Hinnell,
781 and P. A. Ferre, 2014, Surface NMR instrumentation and methods for detecting and
782 characterizing water in the vadose zone, *Near Surf. Geophys.*, 12(2), 271-284,
783 doi:10.3997/1873-0604.2013066.

784 Weichman, P. B., D. R. Lun, M. H. Ritzwoller, and E. M. Lively, 2002, Study of surface
785 nuclear magnetic resonance inverse problems, *J. Appl. Geophys.*, 50, 129–147,
786 doi:10.1016/S0926-9851(02)00135-0.

787 **LIST OF TABLES**

788 *Table 1. The soil hydraulic parameters in Villamblain used in the unsaturated water flow*
789 *model (the Kosugi hydraulic property model).*

790 **FIGURE CAPTIONS**

791 *Figure 1. Schematic presentation of the MRS capacity to measure the water content in water*
792 *saturated porous media. Examples of geological material that correspond to the increasing*
793 *pore size.*

794 *Figure 2. The flowchart of the inverse modeling procedure.*

795 *Figure 3. Location map of the monitoring site. The distance between the MRS loop and the*
796 *borehole 03622X0119/FP3-25 (WGS 84: Lat.-48,00683 m; Long.-1,59130 m) is 76 m.*

797 *Figure 4. a) The annual rainfall recorded in Villamblain between 1995 and 2006. b) The*
798 *groundwater level variations. Gray rectangles show the time interval when the MRS*
799 *monitoring was carried out. c) Daily records of the rainfall and the estimation of the*
800 *Penman potential evapotranspiration during MRS monitoring. d) The cumulative effective*
801 *rainfall (left axis) and the groundwater level (right axis).*

802 *Figure 5. a) Measured amplitude of the MRS signal (color scale) as a function of the pulse*
803 *moment and time. b) Theoretical amplitude computed after the MRS inverse model. c) The*
804 *difference between the measured and the theoretical amplitudes.*

805 *Figure 6. a) The lithological log of the borehole 03622X0119/FP3-25 (Fig. 3). b,c) The water*
806 *content and the relaxation time T_2^* provided by the MRS inverse model. d) The electrical*
807 *resistivity profile.*

808 *Figure 7. a) The water content provided by the MRS inversion. b) The water content*
809 *computed with the HYDRUS-1D program. c) The difference between these two images*
810 *shows a good correspondence in-between. The maximum difference is less than 0.04, and*
811 *the discrepancy is $RMSE = 0.0079$.*

812 *Figure 8. Measured amplitude of the MRS signal versus pulse moment for all soundings*
813 *performed in Villamblain (red dots) and the theoretical amplitude computed after the*
814 *water content provided by the unsaturated water flow model (black line). For each*
815 *sounding, the pulse moment was normalized by the maximum pulse moment over all*
816 *soundings.*

817 *Figure 9. The soil hydraulic functions of the four synthetic layers corresponding to the*
818 *hydraulic parameters shown in Table 1.*

819 *Figure 10. The effective rainfall (black line, left vertical axis) versus time, and the water*
820 *column in the depth interval between 0 and 18 m measured with MRS (gray circles, right*
821 *vertical axis). The gray line shows the water column provided by the water flow modeling.*

822 *Figure 11. The cumulative water column in the unsaturated zone versus depth measured with*
823 *the MRS (solid lines) and that computed with the water flow model (dashed lines). We show*
824 *the results corresponding to the first ($t=0$) and the last ($t=332$ d) days of monitoring. a) The*
825 *cumulative water column. b) The water column versus depth computed with the step of 2 m.*

826